A semi-analytical model for irradiance reflectance in marine and inland waters

J. D. Pravin[1], P. Shanmugam[1,2 *], and Y.-H. Ahn[2]

[1]Ocean Optics and Imaging Laboratory, Department of Ocean Engineering, Indian Institute of Technology Madras, Chennai, 600036, India

[2]Korea Ocean Satellite Research Center, KIOST, Seoul 425-600, Korea

*Corresponding author:

Email: pshanmugam@iitm.ac.in, Phone: 91-44-22574818

Abstract:

A semi-analytical model for predicting irradiance reflectance in turbid and marine and inland waters is developed based on the water-column optical properties and illumination conditions. Irradiance reflectance (R) is the ratio of the upwelling to the downwelling irradiances that can be related to the Gordon's parameter $(b_b/(a+b_b))$ through a proportionality factor 'f'. The conventional assumption of 'f' as a constant (0.33) yields large errors in case of turbid and productive coastal waters, and thus a predictive model based on this assumption is generally restricted to open-ocean waters (low chlorophyll case). In this paper, we have sorted the dependent factors that influence 'f' values in the water column. The parameter 'f' is modeled as a function of wavelength, depth, inherent optical properties (IOPs) and illumination conditions for just below the water surface and throughout the water column. The factors responsible for the variation of R in the water column are also discussed with Hydrolight simulations. Data used for the parameterization and validation are obtained using *in-situ* measurements from clear, turbid and turbid productive waters. Validation reports show good agreement between the model R and *in situ* R values for both marine and inland waters.

1. Introduction

The significance of reflectance is generally well-known as it is the main physical quantity that contains the information regarding the seawater constituents such as phytoplankton, suspended sediments, detrital and dissolved organic matter (Mobley, 1994; Thomas and Stamnes, 2002). Reflectance properties of the seawater constituents vary substantially from one water type to another water type, permitting interpretation of their existence, nature and composition. Moreover, it is used to analyze the directional effects (Gordon et al., 1975; Morel and Prieur, 1977), and is a basic quantity used in remote sensing applications. Reflectance in its basic physical term is defined as the ratio of the incoming and outgoing radiant fluxes and thus it has no unit. It varies between 0 to 1, whereby 0 corresponds to complete transmission and 1 to complete reflection. The reflectance values sometimes go beyond 1 for strongly forward reflecting surfaces such as snow (Painter & Dozier., 2004; Schaepman-Strub et al., 2006). In oceanography, unlike used in other fields, the measured R is not from an ideal diffuse reflector (Lambertian) nor the incident lighting is isotropic. Thus, it is proper to denote this quantity as "irradiance reflectance" rather than "diffuse reflectance". The irradiance reflectance is dependent on the inherent optical properties of the water, but its prediction is very complex. In remote sensing applications, optical properties of the seawater constituents are derived from the reflectance values through inversion models and remote sensing algorithms (Roesler and Perry, 1995; Roesler and Boss, 2003; Shanmugam et al., 2010, 2011; Werdell et al., 2013). Since the reflectance is related to IOPs, the inversion and remote sensing techniques could produce reliable results only if the function 'f' is determined accurately.

Determination of exact R is not easy (Mobley, 2005), as the factor f is not a quantity measured directly with a measuring instrument. The prediction of f is complicated as it depends upon many physical and environmental/illumination conditions (Dev and Shanmugam, 2014b). Several researchers have attempted to sort the dependencies of 'f' in case 1 waters (Gordon et al., 1975; Morel and Gentili, 1993; Morel and Prieur, 1977). The behavior of f in turbid and productive case 2

waters is difficult to predict and there is no general model reported in the literature. Albert and Mobley developed an analytical model to predict R based on the Hydrolight simulations that is limited in case 2 waters (Albert and Mobley, 2003). Though some of the previously published papers show the dependencies of f on solar angle (Kirk, 1984), wind speed (Albert and Mobley, 2003) and IOPs (Hirata and Højerslev, 2008; Loisel and Morel, 2001; Morel and Gentili, 1993; Sathyendranath and Platt, 1997), they do not include a variety of water conditions within coastal and inland environments. Moreover, models accounting the depth-wise variation of R are scarce (Hirata, 2003; Maritorena et al., 1994). Recently, a realistic model of f was reported for a variety of water types and operates as a function of the solar zenith angle, IOPs and wavelength-dependent constants (k_{Chl} and k_{SS}) (Dev and Shanmugam, 2014b). The drawbacks of the existing models that were developed based on radiative transfer simulations are overcome by this model, which is solely dependent on the IOPs and illumination conditions. The objective of the present study is to propose an alternate model without involving any constants and assumptions for predicting the irradiance reflectance in a wide range of marine and inland waters. The irradiance ratio just below the surface ($R(0^-,\lambda)$) and at different depths ($R(\lambda,z)$) is modelled through the function f predicted for just below the surface ($f(0^-,\lambda)$) and at different depths ($f(\lambda,z)$) without relying on any assumptions and wavelength-dependent constants. The calculation of $R(0^-,\lambda)$ requires four inputs namely *Chl* concentration, spectral absorption and backscattering coefficients and solar zenith angle. $R(\lambda,z)$ requires as input the $R(0^-,\lambda)$ (calculated from above four inputs) and vertical diffuse attenuation coefficients $K_u(\lambda,z)$ and $K_d(\lambda,z)$.

2. *In-situ* data

In-situ data were collected on several field campaigns in oceanic and turbid productive coastal waters during May 2012 (Off Point Calimere), August 2013 (Off Chennai), October 2013 (around Chennai coast), November 2013 (Chennai Harbour), May and November 2013 (Muttukaadu lagoon) (Fig. 1). The above field locations are optically different regions characterized by waters with a different composition. Bio-optical measurements were performed on different coastal research

vessels (*CRV Sagar Pachimi, CRV Sagar Purvi and BTV Sagar Manjusha*) allotted by the National Institute of Ocean Technology (NIOT). The radiometric measurements included upwelling and downwelling irradiances from TriOS radiometers and the photometric measurements included absorption and backscattering coefficients from AC-S and BB9 respectively (Dev and Shanmugam, 2014a and 2014b). Measurements were taken approximately 20cm from the sea surface. It is assumed that the IOPs are uniform in the first half meter of the water column from the surface. Note that one cannot measure the radiance or irradiance or any IOPs exactly just below the sea surface due to the wave action. Though the measurements of radiance or irradiance from just below the sea surface (below 20 cm) might contain errors (due to waves and possible titling of instrument), such errors are cancelled out when taking the irradiance ratio to calculate the reflectance values. The AC-S measured absorption and attenuation coefficients were corrected for temperature and salinity effects using the procedure recommended by Sullivan et al., (2006). For scattering error correction, we adopted the Zaneveld et al., (1994) method. Chlorophyll fluorescence and turbidity were measured with a FLNTU sensor. Other ancillary data such as temperature, salinity and conductivity were measured by a CTD sensor.

The nature of water is broadly categorized into five types (based on chlorophyll and turbidity levels as schematically shown in Dev and Shanmugam, 2014b): (i) Type I - Clear water (Off Chennai) (*Chl* < 1 mg m^{-3} and turbidity < 1 NTU), (ii) Type II - Relatively clear water (around Chennai) (1 < *Chl* < 3 mg m^{-3} and 0.5 < turbidity < 3 NTU), (iii) Type III - Relatively turbid water (Chennai Harbour) (5 < *Chl* < 25 mg m^{-3} and 1 < turbidity < 4 NTU), (iv) Type IV - Turbid water (Off Point Calimere) (1 < *Chl* < 3 mg m^{-3} and 3 < turbidity < 14 NTU) and (v) Type V – Productive (eutrophic) water (Muttukaadu lagoon) (*Chl* > 25 mg m^{-3} and turbidity > 5 NTU). Further details on the data acquisition and processing protocols as well as methods for laboratory determination of the water constituents can be found elsewhere (Dev and Shanmugam, 2014a, 2014b; Gokul et al., 2014; Simon and Shanmugam, 2013; Sundarabalan and Shanmugam, 2015).

3. Model description

Theoretically, diffuse reflectance (*R*) is regarded as an apparent optical property (AOP), which is the ratio of the upwelling and downwelling irradiances (Eq. 1). In the field of marine optics and remote sensing, the irradiance reflectance can be calculated analytically from the inherent optical properties (IOP) of the seawater (Eq. 3).

$$R(\lambda, z) = \frac{E_u(\lambda, z)}{E_d(\lambda, z)} \quad (1)$$

$E_{u,d}(\lambda,z)$ at the depth z can be expressed in terms of Beer-Lambert Law as,

$$= \frac{E_u(0^-, \lambda) \times e^{-K_u(\lambda,z)\times z}}{E_d(0^-, \lambda) \times e^{-K_d(\lambda,z)\times z}}$$

$$R(\lambda, z) = R(0^-, \lambda) \times e^{-z[K_u(\lambda,z) - K_d(\lambda,z)]} \quad (2)$$

where,

$$R(0^-, \lambda) = f(0^-, \lambda)\left(\frac{b_b(0^-, \lambda)}{a(0^-, \lambda) + b_b(0^-, \lambda)}\right) \quad (3)$$

Here *R* is related to the IOPs through a factor '*f*' (Gordon et al., 1975; Morel and Prieur, 1977). *a* and b_b denote the absorption and backscattering coefficients respectively, λ the wavelength, 0^- the depth just below the sea surface, and *z* the depth layer from the surface. In the literature, the factor *f* is generally parameterized based on the assumptions applicable to clear oceanic waters and holds very little information of the other water types (such as turbid and productive coastal waters). This limits the possibility of extending such models to predict *R* in coastal and inland waters. In this paper, *f* is determined just below the water surface and at different depths. As the factor *f* is dependent partly on the illumination and environmental conditions, analytic solutions for *f* predictions are not possible (Morel and Gentili, 1991, 1993, 1996). Models with restricted assumptions (such as spectrally invariant, optically homogeneous, zenith sun angle) lower the accuracy of *f* and hence degrade the predicted reflectance values (Sathyendranath and Platt, 1997). However, based on the experiments conducted in different waters we provided meaningful interpretation about this complex *f* factor.

The spectral variation of f is found to have dependency (Loisel and Morel, 2001) on absorption and backscattering coefficients (Eq. 4), whereby its magnitude (S_f+I_f) is dependent on the light field available just below the sea level. The entire factor $f(0^-,\lambda)$ seems to follow a power law where its magnitude is the sum of the solar zenith angle function (S_f) and IOP function (I_f). Plotting the S_f+I_f versus solar zenith angle [Fig. 2(a)], the data points seem scattered when they are shown together for all water conditions. However, it can be closely observed that the trend followed by each water type is rather consistent although having a slight shift among the water types [i.e., Type I (blue) & II (purple) lie at the top, Type III (orange) & IV (pink) in the middle, and Type V (green) at the bottom]. Segregating the magnitude term (S_f+I_f) provides an insight into the variation of each function with the solar zenith angle [Fig. 2(b] and (c)]. The term other than the solar zenith angle function (S_f) that seems to influence the f factor is dependent on the IOPs (I_f). We found the relation between this term (I_f) and the inverse of absorption ($1/a(412)$) based on the interpretation of reflectance properties of different waters. The model requires four surface-measured parameters namely the solar zenith angle, *Chl* concentration, absorption and backscattering coefficients. The coefficients denoted with 0^- represent the surface measurements and λ the spectral function. The $a(412)$ in I_f is the surface measured absorption coefficient at 412nm. The model equation is expressed as follows,

$$f(0^-,\lambda) = \left(S_f + I_f\right) * \left(\frac{b_b(0^-,\lambda)}{a(0^-,\lambda)}\right)^n \tag{4}$$

$$f(0^-,\lambda) = \left\{0.03 * \exp^{(0.0462*\theta_s)} + 0.0671 * \left(\frac{1}{a(412)}\right)^{0.756}\right\} \times \left(\frac{b_b(0^-,\lambda)}{a(0^-,\lambda)}\right)^n \tag{5}$$

where, $n = 0.03 \times \log(Chl) + 0.2243$. (6)

As shown mathematically in Eq. (5) and schematically in Fig. 2(b) and (c), S_f increases exponentially with the increase of solar zenith angle and I_f follows a power function which decreases with increasing $a(412nm)$. The absorption coefficient at 412nm is chosen because significant

variations in the absorption spectra are evident within this spectral region, whereas at longer wavelengths the absorption due to the pure seawater dominates. The wavelength 412 nm has direct applications to remote sensing as most of the ocean color sensors included this band to realize its potential applications. Since the present model corresponds to the reflectance (which contain the information of phytoplankton, mineral particles, detritus and CDOM), choosing a wavelength in the lower blue end can give more accurate information about the water column properties rather than choosing a longer wavelength beyond 500nm. Consequently both the S_f and I_f terms determine the magnitude of $f(0^-,\lambda)$.

Conversely, the term 'backscattering by absorption ratio' (b_b/a) gives the spectral character to $f(0^-,\lambda)$. The spectral slope is governed by the parameter 'n', a function of *Chl* [Fig. 2(d)] (Okami et al., 1982). In case of clear oceanic waters, the spectral slope 'n' is small and thereby produces almost linear $f(0^-,\lambda)$. This is the reason why the case 1 models assume $f(0^-,\lambda)$ as a constant. For productive waters with elevated C*hl* concentrations, the slope causes large spectral variations in $f(0^-,\lambda)$ [Eq. 6]. For clear waters (assuming *Chl* = 0.1 mg m^{-3}), it takes the value of 0.194, and for turbid productive waters (*Chl* = 72 mg m^{-3}), it takes the value of 0.28. The $(b_b/a)^n$ on $f(0^-,\lambda)$ (Eq. 5) is significant due to the combined effect of absorption, fluorescence and backscattering of phytoplankton in the red and NIR regions, particularly at elevated concentrations in productive waters. The high chlorophyll effect is thus accounted in $f(0^-,\lambda)$. Considering all the water types, the predicted S_f+I_f values are in excellent agreement with *in situ* S_f+I_f determinations (Fig. 2(e)).

Irradiance reflectance as a function of depth, $R(\lambda,z)$ can be calculated by combining Eqs. (2) and (3),

$$R(\lambda,z) = f(0^-,\lambda)\left(\frac{b_b(0^-,\lambda)}{a(0^-,\lambda)+b_b(0^-,\lambda)}\right)\times e^{-z[K_u(\lambda,z)-K_d(\lambda,z)]} \quad (7)$$

$$R(\lambda,z) = f(\lambda,z)\left(\frac{b_b(0^-,\lambda)}{a(0^-,\lambda)+b_b(0^-,\lambda)}\right) \quad (8)$$

where, $f(\lambda,z) = f(0^-,\lambda)\times e^{-z[K_u(\lambda,z)-K_d(\lambda,z)]}$. (9)

Clearly, the depth wise *f* function [$f(\lambda,z)$] is largely dependent on the *f* just below the surface [$f(0^-,\lambda)$]. As noted earlier, the $f(0^-,\lambda)$ is a function of light field available at just below the water surface which is approximated on the basis of the solar zenith function and IOPs. In case, if the oceanic water is homogeneous, *R* throughout the water column must be uniform without any fluctuations. This in turn sheds light on the *f* function of both 0^- and *z*. For the uniform *R* throughout the vertical column, $R(0^-,\lambda)$ must be equivalent to $R(\lambda,z)$. Since most of the natural waters are non-homogeneous (because the water constituents are not homogeneously distributed in general) the fluctuations of *R* are expected. The fluctuations in *R* are replicated on the *f*. Since *f* is a function of light field available in the water column, it tends to decrease with depth as denoted by $-z$ (minus *z*) in Eq. 9. The term (K_u-K_d) is the difference in the upwelling and downwelling diffuse attenuation coefficients that induce the corresponding change (increase or decrease) in $f(\lambda,z)$. Thus, any underwater fluctuations in *R* depend on the change in the upwelling and downwelling diffuse attenuation coefficients (Eqs. 7 and 8).

4. Results

For evaluating the performance of the present model, the underwater diffuse reflectance profiles for five water types were modeled based on the measured IOPs (absorption and backscattering) and derived $f(\lambda,z)$ and (K_u-K_d) values. The model *R* values were then compared with those determined from *in-situ* measurements of the upwelling and downwelling irradiances. Figure 3(a_1-e_2) shows the comparison of model-derived and measured reflectances for each water types (Type-I to Type-V), wherein the black line represents the measured *R* and the orange line represents the modeled *R*. Two examples from each water type are presented (in column wise). The sub-plots labeled as *a*, *b*, *c*, *d* and *e* correspond to the water types I to V respectively and the subscripts 1 and 2 represent two different stations for a particular water type. Table 1 provides the further information regarding the total absorption, backscattering coefficients, *Chl* concentration, turbidity and solar zenith angle for all the sub-plots. The *R* spectra of each water type (ranging from clear to turbid) are unique and

distinct in its spectral shape. Figure 3(a_1, a_2) represents the clear oceanic type-I waters with very low chlorophyll concentration (<0.25 mg m^{-3}) and low turbidity (<0.6 NTU). The presence of very low seawater contents diminishes the absorption coefficient in the blue region that subsequently gives high reflectance in this spectral region. At longer wavelengths, high absorption and low backscattering produce very low reflectance. The model is capable of producing the *R* spectra consistent with the *in situ R* spectra. Figure 3(b_1, b_2) represents the relatively clear type-II waters with *Chl* concentration and turbidity less than 2 mg m^{-3} and 2 NTU. Here, the absorption coefficient is relatively higher than that of type-I waters that diminishes the magnitude of the reflectance in the blue region. This is clearly seen with the primary peak shifting from the blue region (Type 1 case) to the green region (around 500-550 nm) due to the absorption effect. Though the *Chl* concentration at these stations is greater than 1 mg m^{-3}, the secondary peak (around 685 nm) is not well pronounced due to the considerable amount of suspended sediments (that increased turbidity level from 1.4 - 2 NTU). The considerable amount of suspended sediments enhances backscattering at longer wavelengths (650-700 nm), resulting in non-zero reflectance. The reflectance spectra predicted by the model agree well with the *in-situ* measurements.

In type-III waters with *Chl* nearly five times greater than its turbidity level, chlorophyll (and of course, other constituents such as colored dissolved substance and non-algal particles) absorbs light strongly in the blue portion, further diminishing the reflectance spectra below 0.01 [Fig. 3(c_1, c_2)]. The reflectance spectra predicted by the model are consistent with the *in-situ* spectra, wherein both the primary and secondary peaks are well pronounced because of the elevated *Chl* concentration and reduced turbidity.

The type-IV waters are dominated by suspended sediments and little chlorophyll in contrast to the type-III waters. The turbidity level at these two stations [Fig. 3(d_1, d_2)] is greater than 5 NTU, while the *Chl* concentration remains low (<2 mg m^{-3}). At these stations, high backscattering by suspended

sediment particles is particularly effected in the NIR region and hence the enhanced *R* values when compared to the previous cases (Types I, II and III). As a consequence, the secondary peak around 685nm is suppressed because of the elevated suspended sediment concentration relative to the *Chl* concentration. The absorption effect of algal and non-algal particles is seen as the reduced *R* in the blue part of the spectrum. The model remains stable and consistent in terms of reproducing the measured *R* spectra.

The applicability of this model is also verified in turbid productive (eutrophic) waters characterized by very high turbidity (>7 NTU) and very high *Chl* (44 mg m^{-3}). The typical *R* spectra from these waters are shown in Fig. 3(e_1, e_2), wherein the primary peak is further shifted toward the yellow spectral region and the secondary peak toward the NIR region. The combined effect of both backscattering and fluorescence/absorption is likely to cause a reflectance peak at NIR (Ahn and Shanmugam, 2007; Dev and Shanmugam, 2014a; Shanmugam et al., 2013). The absorption by phytoplankton, non-algal particles and dissolved substance is abnormally high so that the *R* values approach near-zero (<0.005) in the blue region. Notably, the predicted *R* spectra agree well with the measured *R* spectra in spite of a slight discrepancy in the red portion.

The model consistency to predict the vertical profiles of reflectance is further investigated. Figure 4(a-c) displays the variation of *R* throughout the water column. For brevity, the results are shown only for three different cases that vary vertically due to the IOPs. AOP profile measurements $E_u(\lambda,z)$ and $E_d(\lambda,z)$ may contain possible errors in the near surface (due to the wind-wave action / light focusing / instrument tilt) that it might suffer because of total reflection of upwelling radiation and thus the additional radiance contribution to the downwelling part. To minimize the possible errors due to the wave effects, generally the averaging of AOP/IOP measurements is done throughout the water column. Here, we evaluated the irradiance ratio $R(\lambda,z)$ through Hydrolight simulations to ignore the effects caused by the wind. Depth profiles of chlorophyll and IOPs such as *a*, *c* and b_b

obtained from field measurements were given as inputs (three cases are shown in Fig. 4) and the corresponding irradiance profiles were generated for given wind speed and solar angles. $R(\lambda,z)$ was calculated from the irradiance ratio $E_u(\lambda,z)/E_d(\lambda,z)$ and the vertical diffuse attenuation coefficient (Eq. 10, these parameters are required for Eq. 7 to predict $R(\lambda,z)$).

$$K_{u,d}(\lambda, z_1 \leftrightarrow z_2) = \left(\frac{1}{z_2 - z_1}\right)\left[\ln\left(\frac{E_{u,d}(z_1)}{E_{u,d}(z_2)}\right)\right] \qquad (10)$$

Hydrolight simulations of $R(\lambda,z)$ showed that it obeys the model equation (Eq. 2) and confirms the vertically increasing/decreasing trends in the water column. Note that since the water constituents are not homogeneously distributed with depth, R cannot be constant throughout the water column and can either increase or decrease vertically depending on the constituents present in it (Hirata, 2003; Fig 16 in Sundarabalan and Shanmugam (2015)). Fluctuations in $R(\lambda,z)$ can be accurately predicted by the exponential term 'K_u-K_d' in Eqs. 2 and 7. For example, if $K_u > K_d$, R decreases; if $K_u < K_d$, R increases; or if $K_u/K_d > 1$, R decreases; if $K_u/K_d < 1$, R increases. The value of the diffuse attenuation ratio K_u/K_d, gives the proportionate increase/decrease of R with respect to the reflectance on the layer above. Though K_u and K_d can be derived from IOPs, the present model uses K_u and K_d values from calculated using Eq. 10. Assuming K_u and K_d as a sole function of IOPs ($K_u \sim K_d \sim a+b_b$) would rather lead to a constant R throughout the depth, which is not practically applicable in cases other than homogeneous waters. Thus, the present model of $R(z)$ requires $R(0^-,\lambda)$ (calculated purely from IOPs and incident sun angle) and vertical diffuse attenuation coefficients K_u and K_d.

The Hydrolight input and output profiles for three different stations (row wise) are plotted in Figure. 4(a–c). For brevity the depth profiles of green wavelength are only shown. The depth profiles of *Chl*, *turbidity*, total a, total c and total b_b are the inputs and $E_u(\lambda,z)$, $E_d(\lambda,z)$ are the outputs for given wind speed and solar zenith angles. $K_u(\lambda,z)$, $K_d(\lambda,z)$ and $R(\lambda,z)$ are calculated as discussed above. The non-homogeneous IOP profiles are selected to show the variation of R along the depth. The last column

shows three vertical profiles of (i) Hydrolight derived (direct) R ($R_{HL\text{-}direct}$) (represented in green), (ii) Hydrolight R calculated form the Hydrolight outputs $E_u(\lambda,z)$, $E_d(\lambda,z)$, $K_u(\lambda,z)$, and $K_d(\lambda,z)$ ($R_{HL\text{-}AOP}$) (represented in blue), and (iii) R calculated from the present model (R_{model}). Figure 4(a) shows *Chl* maxima at the surface and decreases rapidly at 3-5 m and then increases at depths greater than 7m. The turbidity also closely follows this trend with an increase and a decrease in the top and bottom layers. A similar trend is replicated in the IOP profiles of a, c and b_b. The K_u and K_d profiles are the function of IOPs following a similar trend but with some additional effects of the light field available at respective depths. It becomes obvious that all the $R(\lambda,z)$ profiles show the variation following the trend of the IOP profiles with a decrease at 3-5 m and an increase at surface and bottom depths. It is also observed that the Hydrolight derived direct R ($R_{HL\text{-}direct}$), smoothly varies according to the IOP profile but fails to account for the variation component associated the f factor at that particular depth. However, the other two R ($R_{HL\text{-}AOP}$ and R_{model}) profiles capture the depth-wise variations accurately; particularly the increase in attenuation at 3-4m is accounted directly on K_u and the subsequent variations are produced in R. It means that the $K_u(\lambda,z)$ and $K_d(\lambda,z)$ have a significant role in influencing the R variation throughout the water column. The fluctuations of R due to the roughened sea state caused by wind are generally restricted to the upper column of the ocean. The three cases shown for three different stations were simulated for zero wind speed. Assuming the wind speed zero avoids the risk of greater (than the actual) downwelling radiances entering the sensor, and thus it is made sure that $K_u(\lambda,z)$ and $K_d(\lambda,z)$ do not contain the unwanted lighting effects other than those influenced by the water column properties. $K_u(\lambda,z)$ and $K_d(\lambda,z)$ as defined in Eq. 10 (as an AOP) can only determine the actual variations of R in the water column. As an IOP or quasi IOP, they would result in the homogeneous behavior of $R(\lambda,z)$ throughout the water column (thus appropriate to predict its variations in the water column). The increase/decrease behavior of R has been discussed in Tables 4, 5, 6 of Dev and Shanmugam (2014b). Figure 4(b) shows another example of increasing and decreasing IOPs and AOPs. In this case, *Chl* decreases toward the depth with slight fluctuations, while turbidity shows well pronounced features - a dip around 5 to 8 m and an increase at depth >

8m because of the presence of considerable amount of inorganic content in the bottom layer. The effects of IOPs and AOPs (K_u and K_d) give rise to the corresponding variations in R – i.e., a decrease at the intermediate layer and an increase at the bottom layer. Note that the $R_{HL\text{-}AOP}$ and R_{model} profiles are better consistent with those of the IOP profiles while the $R_{HL\text{-}direct}$ profile slightly deviates from the IOP profiles due to the missing component. In Fig. 4(c), the IOPs (and both chlorophyll and turbidity) continue to increase toward the depth and the same trend is reflected in AOPs (K_u, K_d) as well. K_u seems to be low when compared to K_d throughout the water column, giving rise to the enhanced $R(\lambda,z)$. Here the $R_{HL\text{-}direct}$ profile is nearly similar to the $R_{HL\text{-}AOP}$ and R_{model} profiles because of the relatively less effect of chlorophyll absorption and more influence of suspended sediment attenuation and backscattering with the increasing depth. These results suggest that the depth-wise R variations can be predictable if $R(0^-,\lambda)$, $K_u(\lambda,z)$ and $K_d(\lambda,z)$ values are calculated correctly. The deduction of the $R(\lambda,z)$ is analytically correct and it is in line with the theory.

Further statistical analysis performed on the spectral and vertical R profile data from the model and measurements (Table 2), demonstrates significantly low errors (RMSE = < 21.4%; MRE = <5.8; Bias = <0.053) and high slope and R^2 values. The one-to-one correspondence with small errors across the entire visible region and depth levels confirms the validity of the present model in a wide range of marine and inland waters. Comparing with the existing models, it should be noted that the existing models are designed with certain assumptions to predict R in case 1 waters or coastal (case 2) waters. For instance, a model that is originally developed for clear oceanic case 1 waters (Gordon et al., 1975; Morel and Prieur, 1977, Kirk, 1984) gives biased reflectance values in turbid coastal and productive water types. A model of case 2 waters (Albert and Mobley, 2003) is restricted to case 2 waters (Dev and Shanmugam, 2014b). Thus, it is more appropriate to compare the results of this study with our previous model since both the models are designed for both marine and inland waters. Figure 5(a)-(d) shows the scatter plots comparing the model R (from the model of Dev and Shanmugam (2014b) and this study) with *in-situ* R for all the water types, where the blue dots

represent the previous model (Dev and Shanmugam, 2014b, denoted as *DS* in Table 3) and the orange dots represent the present model (denoted as *PM* in Table 3) for the key wavelengths 412, 443, 488, 531, 555, 650, 685, 715nm. In Fig. 5(a), results from both the models are nearly identical although the previous model slightly performs better (relative error 18.8%) than the present model (relative error 21.3%). These differences are noticeable in the range below 0.001 where the instrument noise could cause errors in clear oceanic waters when the reflectance values are almost zero in the NIR. In type II relatively clear waters, results from the present model start improving upon those of the previous model (Figure 5(b)), with the relative error of 18.2% for the present model and 15.3% for the previous model. The present model gives better results for the moderately turbid type III waters than the previous model (see the orange dots falling on the 1:1 line in Figure 5(c)). The relative error percentage of the present model is 10.5% when compared to 12.8% for the previous model. In Type IV sediment dominated turbid waters (Figure 5(d)), the present model yields the error percentage of <6% whereas the previous model yields around 21.3%. In the turbid productive type V waters, results from the present model are closer to the *in-situ* data (Figure 5(e)), thereby yielding the relative percentage error of less than 9% over 48% for the previous model. These results suggest that the model is well suited for optically complex coastal and inland waters with high organic and inorganic contents. These validation results clearly emphasize the importance of the present model for predicting *R* in a wide variety of waters without involving the spectral constants with the previous model. The additional parameters with the present model increase its potential and wider applicability.

5. Conclusion

A semi-analytical model has been developed to predict the spectral and vertical profiles of diffuse reflectance in coastal and associated inland waters. The model works a sole function of IOPs and illumination conditions to predict *R*, thereby eliminating its dependency on any assumptions and constant parameters. The results of this model were assessed by comparison with measurement data

and Hydrolight simulations. The model showed its potential in terms of reproducing the measured reflectance profile data with desired accuracy. The present model is applicable to homogenous as well as inhomogeneous waters. Since the model covers a broad range of waters, it can be used to retrieve the optical properties through inversion for clear oceanic waters to turbid eutrophic inland waters. The accuracy may slightly fall in clear oligotrophic waters because of significant errors associated with the instrument noise and residual scattering corrections, however such errors minimal or negligible in turbid and productive waters within coastal and inland environments. Though the present model requires as inputs the $K_u(\lambda,z)$ and $K_d(\lambda,z)$ in addition to IOPs for the calculation of $R(\lambda,z)$, this study enhances our knowledge of the factors contributing to the variation in complex *f* factor throughout the water column. It is anticipated that it will have great significance in hydrologic optics, remote sensing studies, underwater imaging and related engineering applications.

Acknowledgments

This research was supported by INCOIS under the grant (OEC1314117INCOPSHA) of the SATCORE program. The work was partly supported by the Korea Ocean Satellite Centre, Korea Institute of Ocean Science and Technology (KIOST) through support from the Korean Federation of Science and Technology Societies (KOFST), Korea. We would like to thank D. Rajasekhar, The Head, Vessel Management Cell (VMC), and Director of National Institute of Ocean Technology (NIOT) for providing the *CRV Sagar Purvi, CRV Sagar Pachimi and BTV Sagar Manjusha* (Coastal Research Vessels) to Indian Institute of Technology (IIT) Madras, Chennai, India. We sincerely thank the two anonymous reviewers and Topical Editor, Dr. Mario Hoppema, for the valuable comments and suggestions to improve the manuscript.

References

Ahn, Y.-H. and Shanmugam, P.: Derivation and analysis of the fluorescence algorithms to estimate phytoplankton pigment concentrations in optically complex coastal waters, J. Opt. A-Pure Appl. Op., 9, 352–362, doi:10.1088/1464-4258/9/4/008, 2007.

Albert, A. and Mobley, C. D.: An analytical model for subsurface irradiance and remote sensing reflectance in deep and shallow case-2 waters, Opt. Express, 11, 2873–2890, doi:10.1364/OE.11.002873, 2003.

Dev, P. J. and Shanmugam, P.: A new theory and its application to remove the effect of surface reflected light in above-surface radiance data from clear and turbid waters, J. Quant. Spectrosc. Ra., 142, 75–92, doi:10.1016/j.jqsrt.2014.03.021, 2014a.

Dev, P. J. and Shanmugam, P.: New model for subsurface irradiance reflectance in clear and turbid waters, Opt. Express, 22, 9548–9566, doi:10.1364/OE.22.009548, 2014b.

Gokul, E. A., Shanmugam, P., Sundarabalan, B., Sahay, A., and Chauhan, P.: Modelling the inherent optical properties and estimating the constituents' concentrations in turbid and eutrophic waters, Cont. Shelf Res., 84, 120–138, doi:10.1016/j.csr.2014.05.013, 2014.

Gordon, H. R., Brown, O. B., and Jacobs, M. M.: Computed relationships between the inherent and apparent optical properties of a flat homogeneous ocean, Appl. Opt., 14, 417–27, 1975.

Hirata, T.: Irradiance inversion theory to retrieve volume scattering function of seawater, Appl. Opt., 42, 1564–73, 2003.

Hirata, T. and Højerslev, N. K.: Relationship between the irradiance reflectance and inherent optical properties of seawater, J. Geophys. Res., 113, C03030, doi:10.1029/2007JC004325, 2008.

Kirk, J. T. O.: Dependence of relationship between inherent and apparent optical properties of water on solar altitude, Limnol. Oceanogr., 29, 350–356, doi:10.4319/lo.1984.29.2.0350, 1984.

Loisel, H. and Morel, A.: Non-isotropy of the upward radiance eld in typical coastal (Case 2) waters, Int. J. Remote Sens., 22, 275–295, 2001.

Maritorena, S., Morel, A., and Gentili, B.: Di_use reflectance of oceanic shallow waters: influence of water depth and bottom albedo, Limnol. Oceanogr., 39, 1689–1703, doi:10.4319/lo.1994.39.7.1689, 1994.

Mobley, C. D.: Light and Water: Radiative Transfer in Natural Waters, Academic Press, Inc., San Diego, 1994.

Mobley, C. D.: Informal Notes on Reflectances, Sequoia Scientific, Inc, Bellevue, WA 98005, 2005.

Morel, A. and Gentili, B.: Di_use reflectance of oceanic waters: its dependence on Sun angle as influenced by the molecular scattering contribution, Appl. Opt., 30, 4427–4438, 1991.

Morel, A. and Gentili, B.: Di_use reflectance of oceanic waters. II. Bidirectional aspects, Appl. Opt., 32, 6864–6879, 1993.

Morel, A. and Gentili, B.: Di_use reflectance of oceanic waters. III. Implication of bidirectionality for the remote-sensing problem, Appl. Opt., 35, 4850–4862, 1996.

Morel, A. and Prieur, L.: Analysis of variations in ocean color, Limnol. Oceanogr., 22, 709–722, doi:10.4319/lo.1977.22.4.0709, 1977.

Okami, N., Kishino, M., Sugihara, S., and Unoki, S.: Analysis of ocean color spectra (I) – calculation of irradiance reflectance, J. Oceanogr. Soc. Japan, 38, 208–214, 1982.

Painter, T. H. and Dozier, J.: Measurements of the hemispherical-directional reflectance of snow at fine spectral and angular resolution, J. Geophys. Res., 109(D18), D18115, doi:10.1029/2003JD004458, 2004.

Roesler, C. S. and Boss, E.: Spectral beam attenuation coefficient retrieved from ocean color inversion, Geophys. Res. Lett., 30, 1468, doi:10.1029/2002GL016185, 2003.

Roesler, C. S. and Perry, M. J.: In situ phytoplankton absorption, fluorescence emission, and particulate backscattering spectra determined from reflectance, J. Geophys. Res., 100, 13279–13294, doi:10.1029/95JC02176, 1995.

Sathyendranath, S. and Platt, T.: Analytic model of ocean color, Appl. Opt., 36, 2620–2629, 1997.

Schaepman-Strub, G., Schaepman, M. E., Painter, T. H., Dangel, S., and Martonchik, J. V.: Reflectance quantities in optical remote sensing – definitions and case studies, Remote Sens. Environ., 103, 27–42, doi:10.1016/j.rse.2006.03.002, 2006.

Shanmugam, P., Ahn, Y.-H., Ryu, J.-H., and Sundarabalan, B.: An evaluation of inversion models for retrieval of inherent optical properties from ocean color in coastal and open sea waters around Korea, J. Oceanogr., 66, 815–830, 2010.

Shanmugam, P., Sundarabalan, B., Ahn, Y.-H., and Ryu, J.-H.: A New Inversion Model to Retrieve the Particulate Backscattering in Coastal/Ocean Waters, IEEE T. Geosci. Remote, 49, 2463–2475, doi:10.1109/TGRS.2010.2103947, 2011.

Shanmugam, P., Suresh, M., and Sundarabalan, B.: OSABT: An innovative algorithm to detect and characterize ocean surface algal blooms, IEEE J. Sel. Top. Appl., 6, 1879–1892, 2013.

Simon, A. and Shanmugam, P.: A new model for the vertical spectral diffuse attenuation coefficient of downwelling irradiance in turbid coastal waters: validation with in situ measurements, Opt. Express, 21, 30082, doi:10.1364/OE.21.030082, 2013.

Sullivan, J. M., Twardowski, M. S., Zaneveld, J. R. V, Moore, C. M., Barnard, A. H., Donaghay, P. L. and Rhoades, B.: Hyperspectral temperature and salt dependencies of absorption by water and heavy water in the 400-750 nm spectral range., Appl. Opt., 45(21), 5294–309, 2006.

Sundarabalan, B. and Shanmugam, P.: Modelling of underwater light fields in turbid and eutrophic waters: application and validation with experimental data, Ocean Sci., 11, 33–52, doi:10.5194/os-11-33-2015, 2015.

Thomas, G. E. and Stamnes, K.: Radiative Transfer in the Atmosphere and Ocean, Cambridge University Press, 73–77, 2002.

Werdell, P. J., Franz, B. A., Bailey, S.W., Feldman, G. C., Boss, E., Brando, V. E., Dowell, M., Hirata, T., Lavender, S. J., Lee, Z., Loisel, H., Maritorena, S., Mélin, F., Moore, T. S., Smyth, T. J., Antoine, D., Devred, E., d'Andon, O. H. F., and Mangin, A.: Generalized ocean color inversion model for retrieving marine inherent optical properties, Appl. Opt., 52, 2019–2037, doi:10.1364/AO.52.002019, 2013.

Zaneveld, J. R. V., Kitchen, J. C. and Moore, C.: Scattering error correction of reflecting-tube absorption meters, in Ocean Optics XII, vol. 26, pp. 44–55, International society for Optics and Photonics, 1994.

Table 1. Information regarding the optical properties and illumination conditions for those samples presented in Fig. 3.

Water Type	*Figure 3*	*a*(412) (m^{-1})	b_b(412) (m^{-1})	*Chl* (mg m^{-3})	*Turbidity* (NTU)	*Solar zenith angle* (deg)
Type I	a_1	0.129	0.0154	0.2	0.59	41.15
	a_2	0.132	0.016	0.23	0.6	25.52
Type II	b_1	0.385	0.0481	1.99	2.03	33.59
	b_2	0.493	0.0325	1.68	1.43	39.47
Type III	c_1	1.234	0.0383	17.72	1.86	42.38
	c_2	1.183	0.0471	16	2.23	53.8
Type IV	d_1	0.928	0.232	1.25	8.66	19.39
	d_2	0.56	0.1467	1.09	5.64	31.92
Type V	e_1	8.1	0.29	49.28	7.66	20.94
	e_2	6.56	0.24	44.64	7.79	54.91

Table 2. Statistical comparison of the model and *in-situ R* for five types of waters.

λ	*RMSE*	*MRE*	*Bias*	*Slope*	*Intercept*	R^2
412	0.214	-0.012	-0.024	0.772	-0.466	0.829
448	0.185	-0.018	-0.033	0.851	-0.305	0.86
488	0.17	-0.022	-0.038	0.908	-0.188	0.839
531	0.154	-0.02	-0.03	0.928	-0.139	0.777
555	0.148	-0.018	-0.027	0.922	-0.14	0.755
670	0.181	-0.025	-0.053	0.955	-0.144	0.849
685	0.214	-0.058	-0.121	1.023	-0.075	0.846
710	0.197	-0.006	-0.013	0.995	-0.024	0.897

Table 3. Relative differences between the model *R* from the previous work of [a]Dev and Shanmugam, 2014b (DS) and this study (present model - PM) and the in-situ *R* for the five water types.

		412	448	488	531	555	670	685	710	*average*
Type I	*PM*	0.277	0.081	0.113	0.242	0.274	0.242	0.033	0.445	0.213
	DS[a]	0.035	0.127	0.009	0.139	0.137	0.13	0.315	0.52	0.188
Type II	*PM*	0.215	0.239	0.17	0.181	0.171	0.191	0.266	0.021	0.182
	DS[a]	0.085	0.083	0.139	0.139	0.157	0.172	0.169	0.28	0.153
Type III	*PM*	0.23	0.16	0.072	0.028	0.011	0.028	0.163	0.145	0.105
	DS[a]	0.044	0.087	0.114	0.108	0.111	0.164	0.153	0.243	0.128
Type IV	*PM*	0.127	0.011	0.038	0.009	0.006	0.113	0.13	0.008	0.055
	DS[a]	0.178	0.197	0.177	0.2	0.196	0.22	0.254	0.279	0.213
Type V	*PM*	0.167	0.09	0.017	0.071	0.051	0.067	0.201	0.035	0.087
	DS[a]	0.125	0.368	0.542	0.312	0.619	0.674	0.619	0.639	0.487

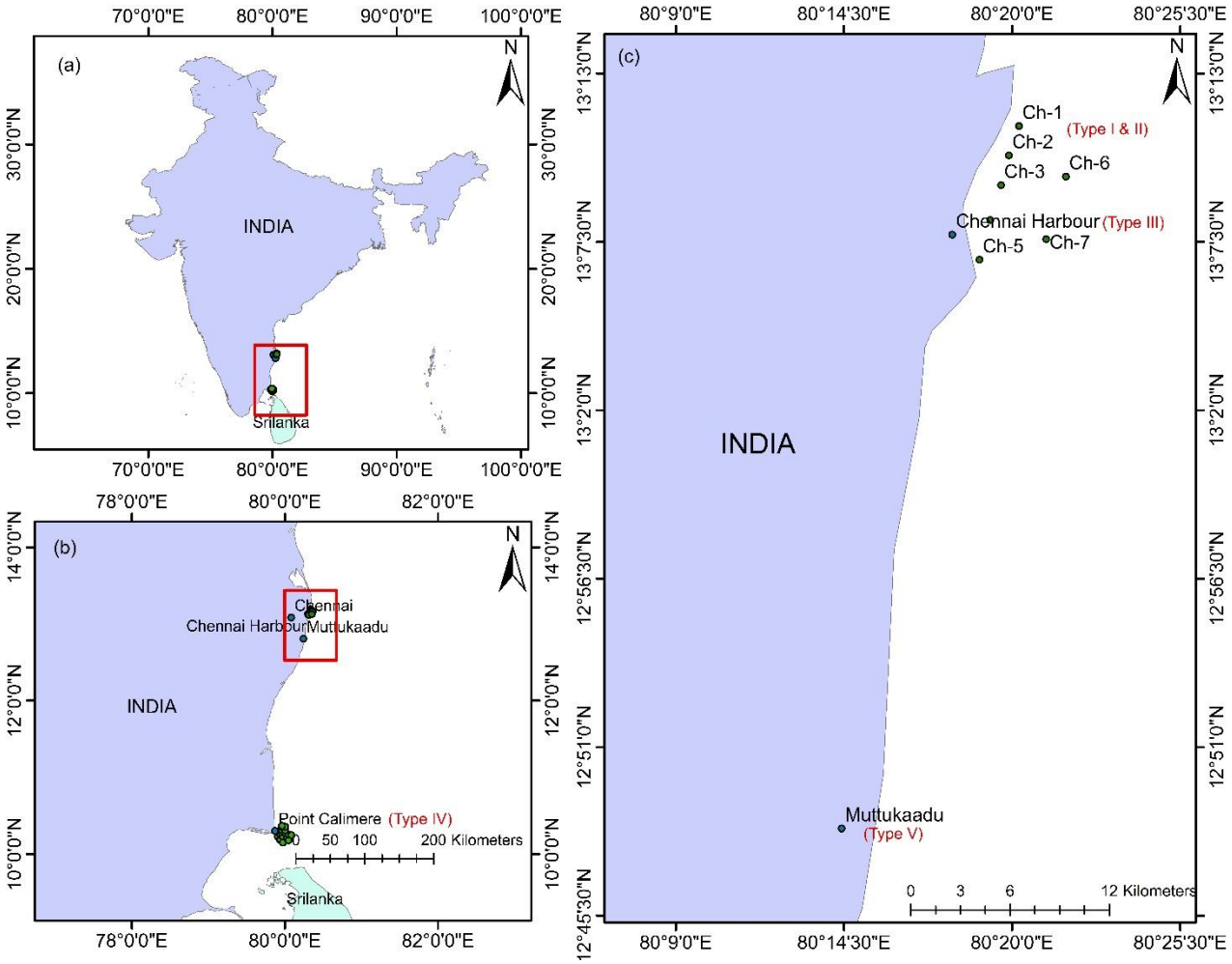

Figure 1(a). Study sites on the southeast part of India (shown in red box). **(b)** Magnified study area covering Chennai, Muttukadu and Point Calimere. **(c)** Magnified study area with stations covering Chennai (Type I, II, and III) and productive Muttukaadu lagoon system (Type V).

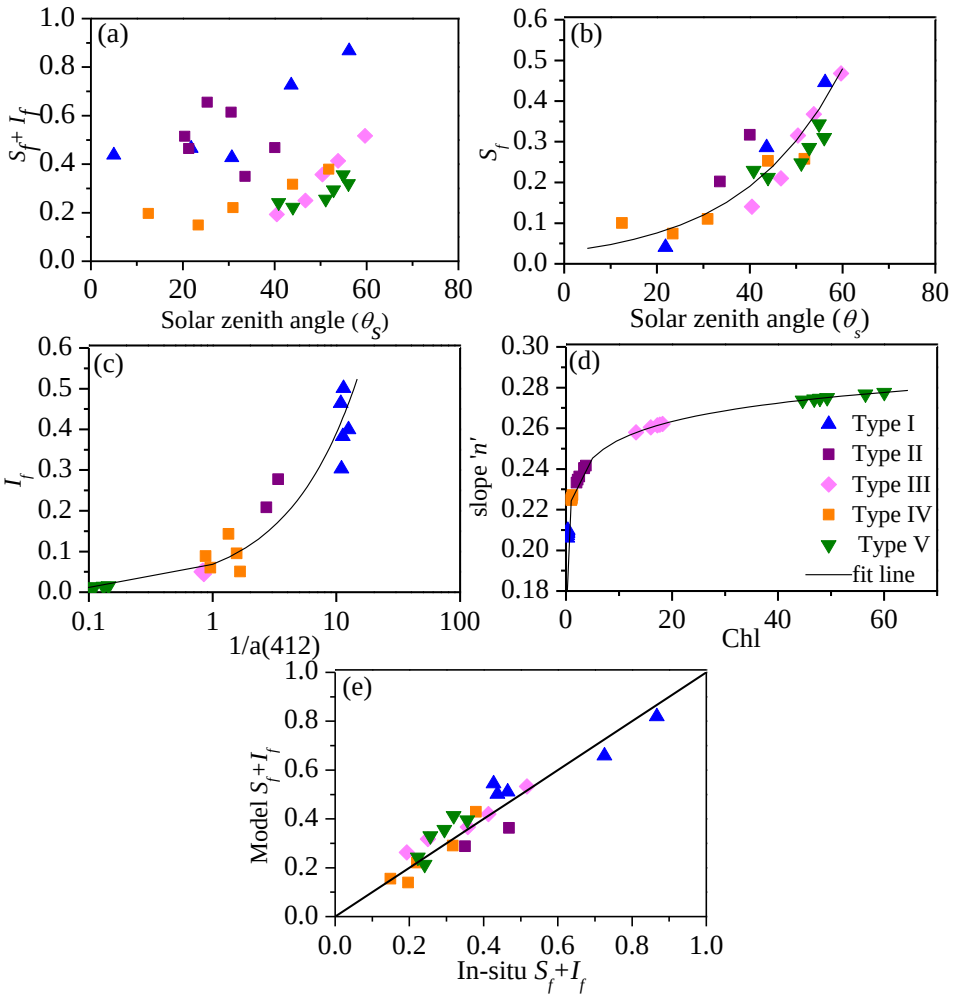

Figure 2. Scatter plots showing dependencies of (a and b) S_f on the solar zenith angle, (c) I_f on the *1/a*(*412*), (d) *Chl* on the spectral slope parameter '*n*' and (e) 1:1 correspondence of model and *in situ* S_f and I_f.

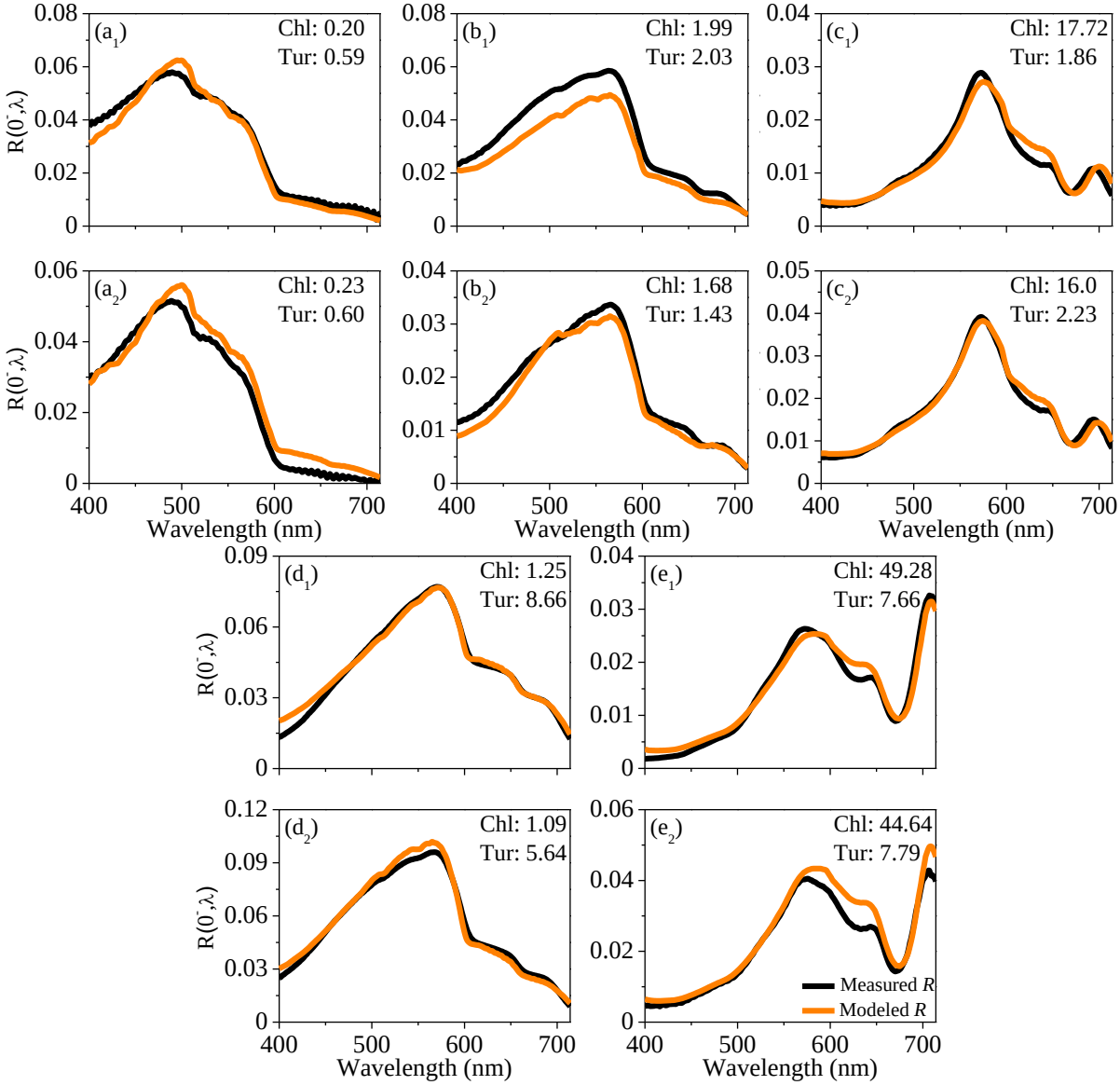

Figure 3. Comparison of the modeled *R* (orange line) and measured *R* (black line) from different waters. Two examples of each water type (a_1,a_2)-type I, (b_1,b_2)-type II, (c_1,c_2)-type III, (d_1,d_2)-type-IV, (e_1,e_2)-type V are presented. (More information on the IOPs, please refer Table. 1).

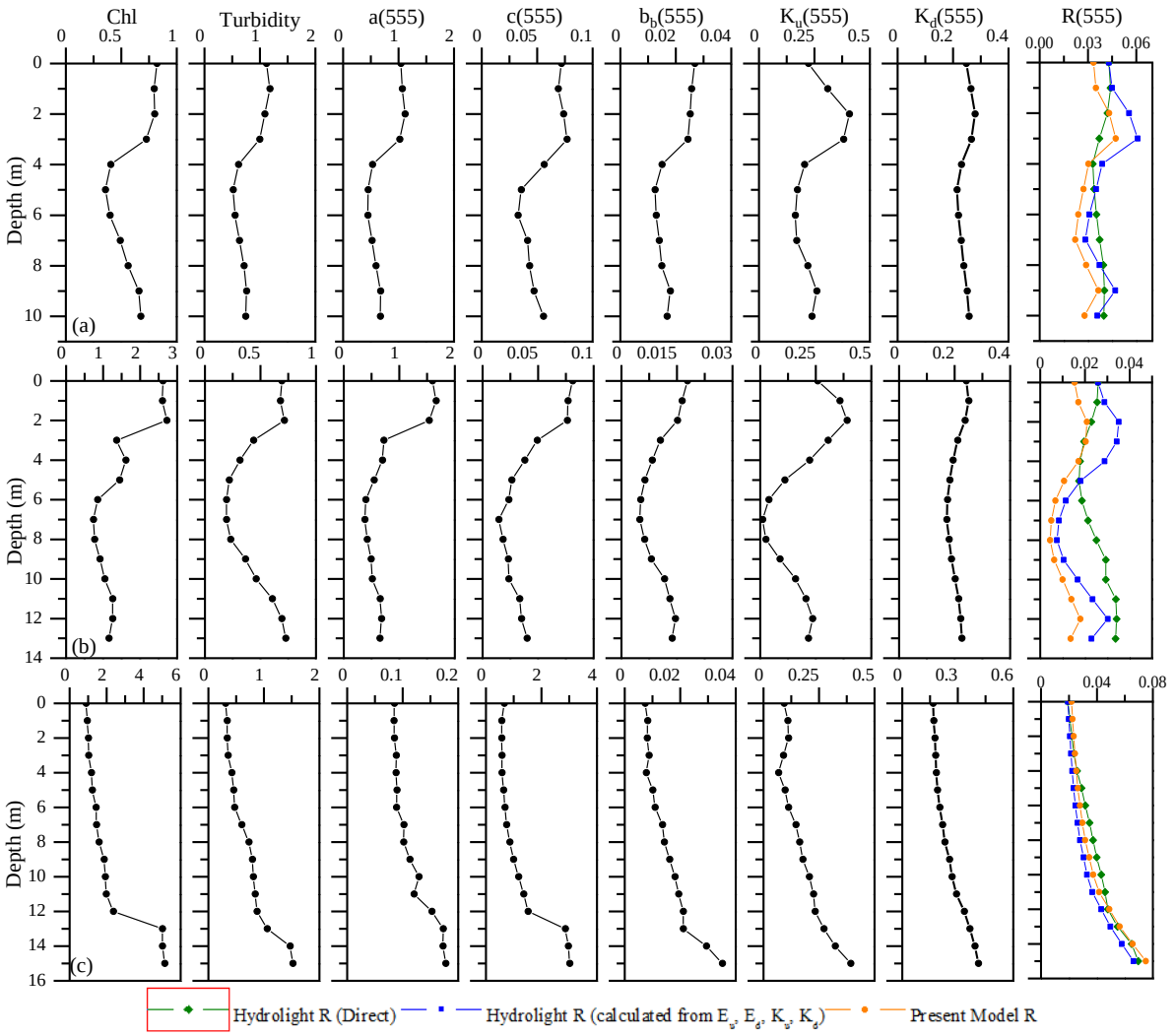

Figure 4. Vertical profiles of the *Chl*, *turbidity* and IOPs (total $a(555,z)$, $c(555,z)$, $b_b(555,z)$) for three different stations (considered as input for Hydrolight simulations) and the corresponding output profiles $K_u(555,z)$, $K_d(555,z)$ and $R(555,z)$. Last column represents Hydrolight direct R, $R_{HL\text{-}direct}$ (Green line), Hydrolight R calculated from E_u, E_d, K_u and K_d, $R_{HL\text{-}AOP}$ (blue line) and the present model, R_{model} (orange line).

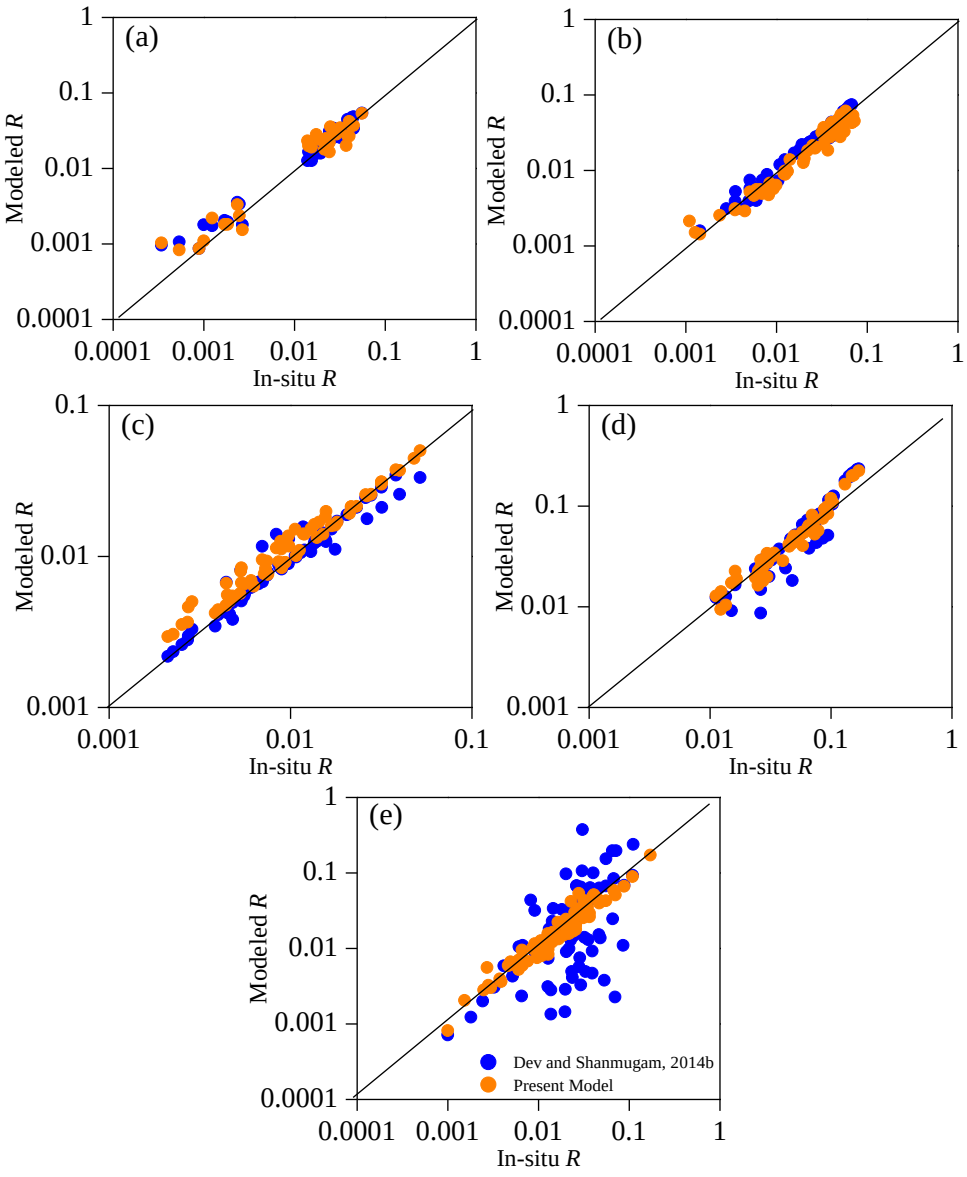

Figure 5. Scatter plots comparing the *R* values from the present and previous models and *in-situ R* for **(a)** type I, **(b)** type II, **(c)** type III, **(d)** type IV and **(e)** type V waters respectively. (Blue dots represent Dev and Shanmugam (2014b) and orange dots represent present model).